**Earth, Planets and Space**

**FULL PAPER**

**Open Access**

# Longitudinal structure in electron density at mid-latitudes: upward-propagating tidal effects

Hui Wang[*] and Kedeng Zhang

**Abstract**

This work studies the upward-propagating migrating and non-migrating tidal effects from the lower atmosphere on the longitudinal variation of electron density ($\Delta Ne$) in both the E and F regions at mid-latitudes during the 2002 March equinox. A total of 12 runs are conducted using the Thermosphere Ionosphere Electrodynamic General Circulation model for theoretical investigation. The $\Delta Ne$ at altitudes above 200 km is affected by upward-propagating tides, with maximum values attained around 300 km. Migrating tides result in reduced longitudinal differences in the $\Delta Ne$ over North America and in the Southern Hemisphere, while non-migrating tides induce a wave-4 pattern in both hemispheres. The non-migrating effect is weaker than the migrating effect after penetrating into the F region. The neutral composition (i.e., ratio of atom oxygen to molecular nitrogen) is dominant in regulating the $\Delta Ne$ in both the migrating (accounting for approximately 64%) and non-migrating (about 60%) tidal penetration processes. The $\Delta Ne$ caused by the tidal meridional wind (accounting for approximately 70%) is stronger than the tidal zonal wind (about 30%) under both the migrating and non-migrating tidal conditions, except in the Southern Hemisphere under migrating tidal input. This work contributes to our understanding of the mechanisms for the longitudinal modulation of the $\Delta Ne$ at mid-latitudes.

**Keywords:** Mid-latitude ionosphere, Electron density, Longitudinal variation, Lower atmospheric tides, TIEGCM model

## Background

The equatorial lower atmosphere is coupled to the F region ionospheric electron density ($Ne$) (England 2012). A prominent wave-4 longitudinal structure is reported by a number of satellite observations (Sagawa et al. 2005; Immel et al. 2006; England et al. 2006b; Lin et al. 2007; Lühr et al. 2007; Kil et al. 2008, 2015; Pedatella et al. 2008; Scherliess et al. 2008; Wan et al. 2008; Liu et al. 2009; Kwak et al. 2012) and simulations (Hagan et al. 2007; Jin et al. 2008; Ren et al. 2010). These wave-4 structures are believed to be caused by the non-migrating DE3 tide (Hagan and Forbes 2002; Henderson et al. 2005; Sagawa et al. 2005; England et al. 2006a; Immel et al. 2006). When the DE3 E layer wind dynamo electric field is mapped to the F layer, it causes DE3 changes in the electron density through vertical transport processes. The annual and seasonal variations of DE3 are similar to those of ionospheric parameters, which support the E-F layer electric field coupling mechanism (Lin et al. 2007; Kil et al. 2008; Wan et al. 2008; England et al. 2009; Fang et al. 2009; Oberheide et al. 2009; Häusler and Lühr 2009; Mukhtarov and Pancheva 2011; Brahmanandam et al. 2011; Wu et al. 2012; Pedatella et al. 2012; Nogueira et al. 2013).

Whether or not the lower atmosphere is closely coupled to the mid-latitudinal ionosphere is still not well understood. Previous regional and global observations have disclosed prominent wave-2 and wave-1 longitudinal structures of the $Ne$ in the F layer in the Northern and Southern Hemispheres (Zhang et al. 2011; Zhao et al. 2013; Xu et al. 2013; Wang et al. 2016). Wang et al. (2016) found a wave-1 longitudinal structure of $Ne$ existing in the E layer in both hemispheres. The longitudinal variation of thermosphere and ionospheric parameters

*Correspondence: h.wang@whu.edu.cn
Department of Space Physics, School of Electronic Information, Wuhan University, Wuhan, Hubei, China

are often related to non-migrating tides, either generated in situ or upward-propagated from the lower atmosphere (Wu et al. 2012). A recent model study by Wang et al. (2015) quantitatively investigates in situ physical processes in F regions in association with the wave-2 and wave-1 longitudinal structure of the *Ne*. It shows that the vertical motion of plasma, caused by the zonal wind, accounted for 80% of the wave-2/wave-1 variations in *Ne* in the Northern/Southern Hemisphere. Meridional wind, neutral composition, and solar heating are responsible for the remnant. In the E layer, the dominant in situ process is solar heating (Wang et al. 2016). These results indicate that local/in situ physical processes contribute to observed longitudinal variations of *Ne* in both the E and F regions and can compromise the model–observation differences. However, the roles of upward-propagating migrating and non-migrating tides from the lower atmosphere are still not well understood and need further investigation. Wang and Liu (2015) revealed that the longitudinal differences of the F region's *Ne* over NA were enhanced by 15% when migrating tidal inputs were turned on at the model's low boundary. But its effect on the E region's *Ne* was not discussed.

The aim of this work is to examine, in detail, the upward-propagating tidal effect from the lower atmosphere on the ionospheric *Ne* using the National Center for Atmospheric Research's (NCAR) TIEGCM (Heroux and Higgins 1977). In the following section, the phrase 'tides' means those that originate from the lower atmosphere. The questions that we want to address here are: (1) what is the role of the lower atmosphere tides in the E and F regions? (2) how do lower atmosphere tides affect the low and upper ionosphere? Various researchers have studied tidal effects on ionospheric parameters at equatorial regions using the TIEGCM model. (Heroux and Higgins 1977; Heroux and Hinteregger 1978; Heelis et al. 1980; Dickinson et al. 1984; Emery et al. 2008; Wu et al. 2012). With respect to the mid-latitudes, several recent model and observational studies showed that for manifesting the mid-latitude summer night anomaly, tidal components such as DE1 and DW2 in combination with SPW1 are predominant in the Northern Hemisphere, whereas D0 in combination with SPW1 are the major components in the Southern Hemisphere (Chen et al. 2013; Jones et al. 2013; Xiong and Lühr 2014; Chang et al. 2015). However, origins of these non-migrating tides, especially the quantitative contribution from the lower atmosphere, are not completely understood.

## Model and observation
### TIEGCM
TIEGCM is a three-dimensional time-dependent model of the coupled thermosphere and ionosphere. It consistently solves ion continuity, momentum, and energy equations. The TIEGCM model is driven by a high-latitude electric field (Heelis et al. 1982), solar EUV, and UV spectral fluxes parameterized by the F10.7 index (Richards et al. 1994), and tides (global scale wave model) at the low boundary (Hagan and Forbes 2002). Its outputs are global winds, plasma and neutral temperatures, and densities.

The horizontal resolution of the model is set to be 2.5° by 2.5° in geographic longitude and latitude, respectively. There are 57 pressure surfaces extending from 97 km to about 700 km (depending on the solar activity) with a vertical resolution of a quarter scale height. All simulations are run for the 2002 March equinox. The input parameters are: hemispheric power = 39 GW, cross-polar cap potential = 60 kV, and F10.7 = 200 sfu. The model is run for 48 h to reach a quasi-steady state and then continued from the start-up simulation for another 24 h; these data are used for analysis. The electron density is sorted into geographic longitude and magnetic local time (MLT) bins with a resolution of 15° in longitude and 1 h in MLT. The longitudinal mean value is subtracted from each MLT sector to better explore the quantity's longitudinal variation. The study focuses on the mid-latitudes between ±40° and ±60° magnetic latitude (MLat). We run the TIEGCM model, separately with and without migrating tides (sun-synchronous) and non-migrating tides (longitude dependent) imposed at the lower atmosphere, in order to study the tidal effects on *Ne*. The tidal amplitudes vary considerably depending upon the season at mid-latitudes in the MLT (e.g., Laskar et al. 2016). The tidal components in March are specified by GSWM-02 including both the diurnal and semidiurnal harmonics.

### Global scale wave model (GSWM)
GSWM is a two-dimensional, linearized, steady-state model. It solves the extended Navier–Stokes equations for tidal and planetary wave perturbations as a function of latitude and altitude for a specified zonal wave number and periodicity (refer to http://www.hao.ucar.edu/public/research/tiso/gswm/gswm.html for additional details). GSWM-02 is used in TIEGCM model (Hagan and Forbes 2002, 2003). GSWM-00 includes monthly variable migrating tidal results in response to solar radiation. GSWM-02 includes both GSWM-00 results and the migrating and non-migrating diurnal and semidiurnal tides that are excited by latent heat release due to tropical deep convection, and offers monthly outputs. GSWM-02 provides 13 diurnal and semidiurnal tidal components, such as standing diurnal and semidiurnal tidal components as well as eastward and westward propagating harmonics with wave numbers from 1 to 6 (W6-E6).

Oberheide et al. (2006) performed a comprehensive study by comparing non-migrating tidal components

from GSWM-02 with those from TIDI measurements of zonal and meridional winds in the mesosphere/lower thermosphere on board TIMED. Monthly averaged amplitude and phase for seven tidal components are presented at altitudes between 85 and 105 km. A comparison of the results indicates that there is good quantitative agreement between TIDI and the model predictions during equinox, but the latter tend to underestimate the westward 2 diurnal tide and standing diurnal tide during solstice. For westward 2 and standing diurnal tidal forcing, both latent heating and planetary wave/migrating tidal nonlinear interactions are equally important. As a linear tidal mode, the GSWM cannot account for nonlinear processes, such as planetary wave/migrating tidal interaction forcing.

### CHAMP

CHAMP had a near-polar (83.7° inclination) orbit (Reigber et al. 2002). The Planar Langmuir Probe (PLP) on board CHAMP measured the electron density every 15 seconds. Data, from 2002 and 2003, were selected representing high solar activity. A length of 131 days, centered on the March equinox, is chosen in order to cover the full local time cycle for CHAMP. The magnetic local time hours were covered on different days, but because the data being considered cover 2 years, local time seasonal correlation was somewhat smeared out. The study focused on the mid-latitudes between 40° and 60° MLat. We presented the results in magnetic latitude and magnetic local time because, for a given geographic latitude, the electron density showed a significant longitudinal dependence due to the tilt of the Earth's dipole axis. This dependence was greatly removed by using magnetic coordinates. The electron density was sorted into geographic longitude and MLT bins with a resolution of 15° longitude and 1 h in MLT. The longitudinal mean value was subtracted from each MLT sector to better explore the quantity's longitudinal variation.

## Results and discussion

### Data–model comparison

The simulated $\Delta Ne$ is compared with the CHAMP satellite observations at 400 km altitude. The longitudinal and magnetic local time variations of the CHAMP $\Delta Ne$ in the Northern (left) and Southern (right) Hemispheres are shown in Fig. 1. In observations, there exist a wave-2 structure (one peak and trough over NA (180°W−0°), another peak and trough over the Europe-Asia sector (0°−180°E) in the Northern Hemisphere), and a wave-1 structure (one peak and trough) in the Southern Hemisphere. Both peaks and troughs shift eastward as the local time increases. The wave amplitudes are larger in the Southern than in the Northern Hemisphere. Wang
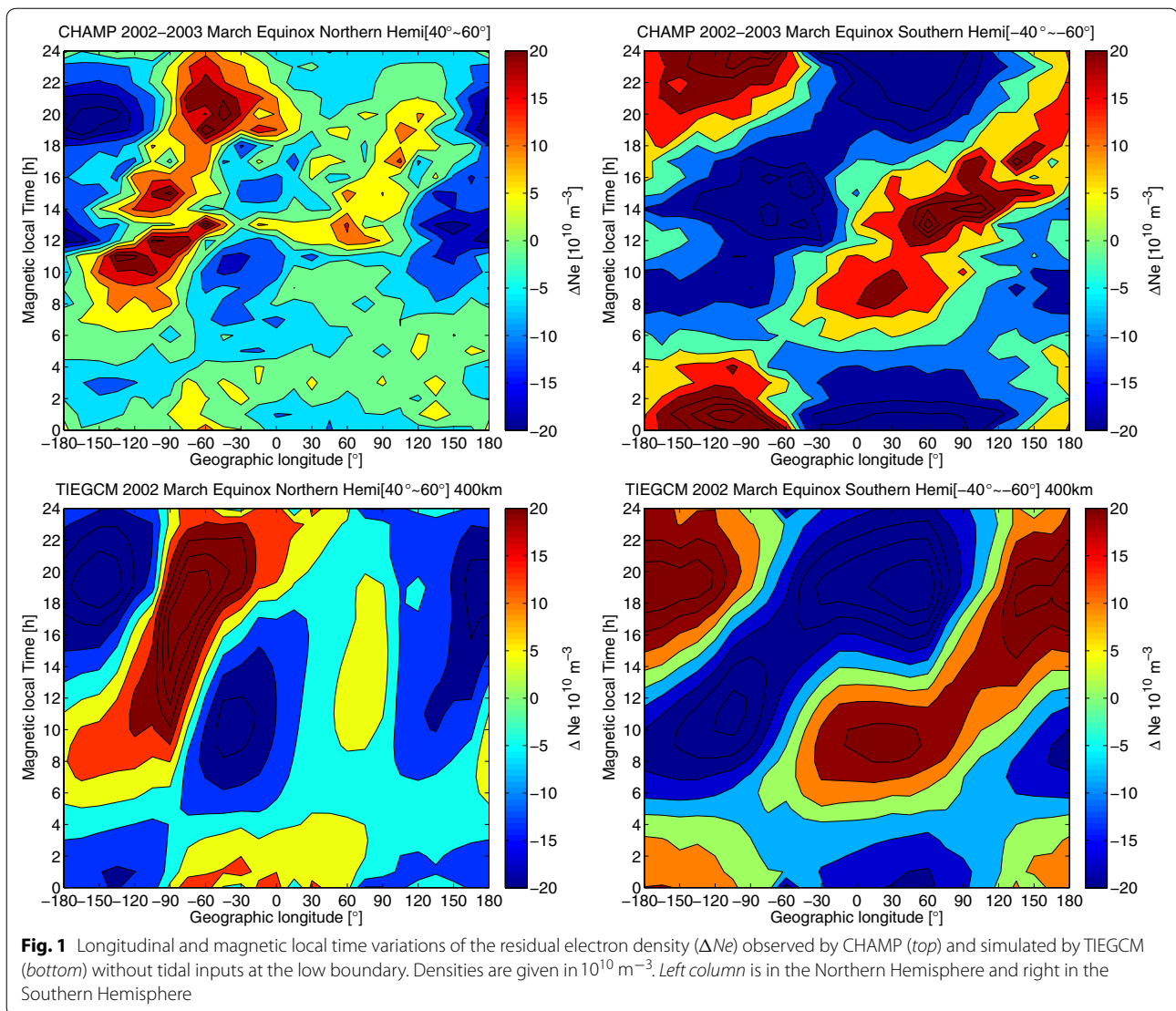
et al. (2016) showed that such longitudinal and diurnal features existed throughout the whole year and for all solar activity levels. Wang and Liu (2015) indicated that local physical processes (i.e., thermospheric neutral wind and solar heating) contributed to the observed longitudinal structure of the *Ne*.

The TIEGCM simulated $\Delta Ne$ is shown at the bottom of Fig. 1. Here, the lower atmospheric tides are not added; therefore, the model's results represent in situ processes. These results are generally consistent with observations in large-scale structures, showing obvious wave-2 and wave-1 longitudinal patterns in the Northern and Southern Hemispheres. The hemispheric and local time asymmetries are also well reproduced by the model. These affirm that the model can be used for theoretical studies. Some small-scale structures are not reproduced by the model, which might be due to the fact that the model is a 1-day result with 131-day averaged solar wind and IMF parameters as input, while the observations are an accumulation of results over 131 days, as well as due to the fact that the tidal effects are not included in the model.

### Migrating tidal effects

When migrating tides are imposed at the lower boundary of TIEGCM, the simulated $\Delta Ne$ is shown at the top of Fig. 2. The longitudinal and local time distribution of the $\Delta Ne$, with migrating tide as inputs, are almost the same as those without migrating tides (see the bottom of Fig. 1). The residual $\Delta Ne$, due to migrating tides, which is the focus of this research, is shown at the bottom of Fig. 2. They are the difference between the $\Delta Ne$ with and without migrating tidal forcing (i.e., the top of Fig. 2, minus the bottom of Fig. 1). There is a wave-1 structure in both the Northern and Southern Hemispheres. In the Northern Hemisphere, the structure is relatively weak, in comparison with the Southern Hemisphere. The northern wave pattern, produced by the upward-propagating migrating tide, is almost out of phase with the wave structure produced by in situ processes, while the southern wave pattern is out of phase relation in the pre-noon and in-phase relation in the post-noon period (compare Fig. 2 with Fig. 1, bottom). Therefore, the migrating tide reduces (increases) the wave amplitude caused by in situ processes in the Northern (Southern) Hemisphere. The tidal effect is stronger in the Southern rather than the Northern Hemisphere.

The altitudinal and longitudinal variations of the residual $\Delta Ne$ at 14 MLT are shown in Fig. 3, to demonstrate the tidal effects at E and F regions. The longitudinal absolute differences in the $\Delta Ne$ (top panel) are negligible at altitudes below 200 km, which is due to relatively lower density at the E region in comparison with that at F region. When looking at the relative differences (bottom
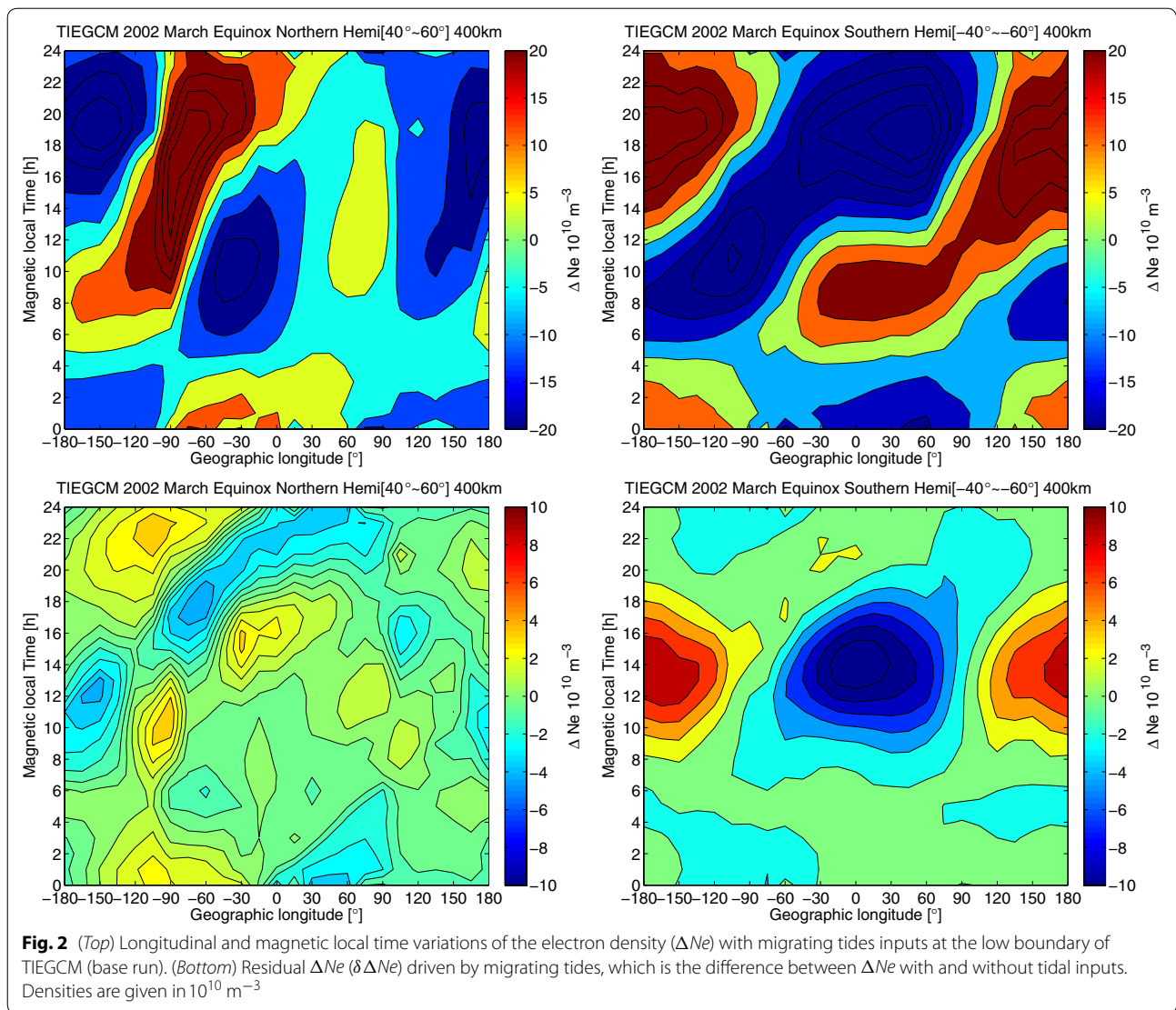
**Fig. 1** Longitudinal and magnetic local time variations of the residual electron density (Δ*Ne*) observed by CHAMP (*top*) and simulated by TIEGCM (*bottom*) without tidal inputs at the low boundary. Densities are given in $10^{10}$ m$^{-3}$. *Left column* is in the Northern Hemisphere and right in the Southern Hemisphere

panel), the longitudinal variations are quite comparable at altitudes below 200 km and above 200 km. The amplitudes of the longitudinal absolute differences reach a maximum at altitudes of around 300 km and then decrease with increasing altitudes. It is interesting to note that the longitudinal structure does not change significantly with altitude. The tidal effects at both the E and F layers indicate the upward propagation of tides from the lower atmosphere into the thermosphere.

The next question is how the migrating tide affects the F layer *Ne*. We classify the tidal effects into two categories: tidal wind and tidal non-wind effects. As suggested by previous theoretical and model works at equatorial regions (Lühr et al. 2007; Jin et al. 2008; Brahmanandam et al. 2011; Pedatella et al. 2012; Ren et al. 2009; England et al. 2010; Zhang et al. 2010; Oberheide et al.

2011), lower atmosphere tides could penetrate directly into the thermosphere, leading to an ionospheric longitude variation driven by in situ changes in neutral winds (i.e., tidal wind effect) or neutral composition (i.e., tidal non-wind effect), in addition to the E-F electric field coupling mechanism. In order to investigate the tidal effects, we run the TIEGCM under six conditions: (1–3) without migrating tidal input, and with zero zonal or meridional or neutral wind; (4–6) with migrating tides, and with zero zonal or meridional or neutral wind. A comparison of those results enables us to discern the function of tidal wind and tidal non-wind. For example, the difference between one run without tide and one run without tide together with zero zonal wind shows in situ zonal wind effect. The difference between one run with tide and one run with tide together with zero zonal wind shows both
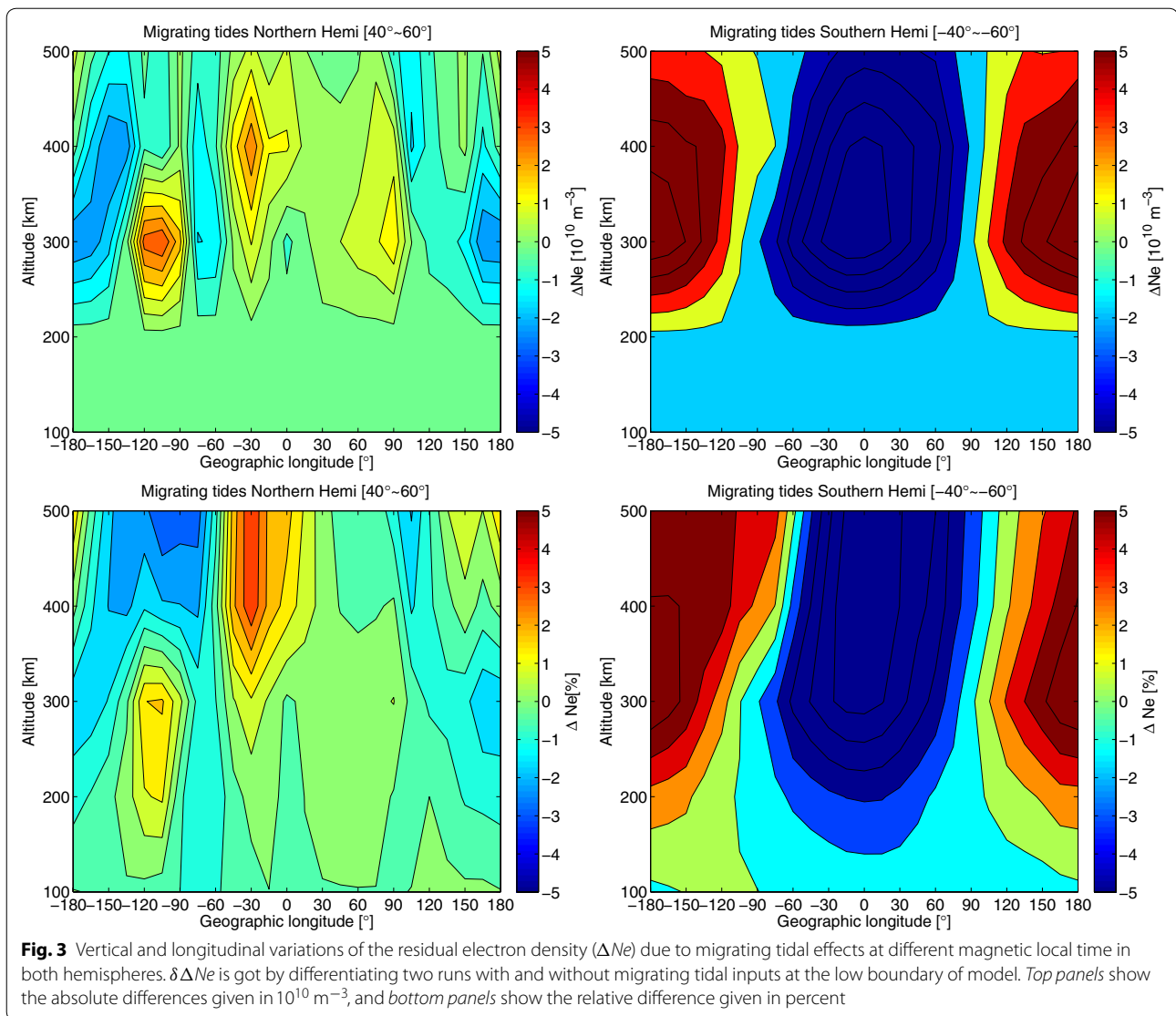
**Fig. 2** (*Top*) Longitudinal and magnetic local time variations of the electron density (Δ*Ne*) with migrating tides inputs at the low boundary of TIEGCM (base run). (*Bottom*) Residual Δ*Ne* (δΔ*Ne*) driven by migrating tides, which is the difference between Δ*Ne* with and without tidal inputs. Densities are given in $10^{10}$ m$^{-3}$

the in situ and tidal zonal wind effects. By further differentiating these two results, we can separate the tidal zonal wind effect from the in situ zonal wind effect.

Figure 4 shows the tidal wind effect, where from top to bottom the tidal zonal wind ($U_y$), meridional wind ($U_x$), and neutral wind are pictured. The tidal zonal wind results in both a wave-2 and wave-1 structure of the Δ*Ne* in the Northern and Southern Hemispheres. Different from the in situ processes, as presented in Fig. 1, the wave structure does not significantly change with the magnetic local time. Therefore, they are in phase with those induced by in situ processes in the pre-noon sector, while out of phase in the post-noon sector.

The tidal wind effects are believed to work through the vertical transport of plasma. Figure 5 shows the meridional (top) and zonal (bottom) winds due to migrating

tides. The tidal meridional wind is poleward, from early morning to pre-noon, and equatorward in the other local time. The tidal zonal wind is westward in the pre-noon and evening sectors, while weakly eastward in the post-noon sectors.

The vertical velocity due to neutral winds is shown in Fig. 6, separately for the zonal wind ($V_y$), meridional wind ($V_x$), and neutral wind ($V_y + V_x$). The plasma vertical velocity $\Delta V_y$ driven by tidal zonal wind is shown at the top of Fig. 5: $V_y = U_y \sin D \cos |I| \sin |I|$, where $U_y$ is the tidal zonal wind, $D$ is magnetic declination, $I$ is the magnetic inclination angle, and $D$ and $I$ are derived from IGRF model. In the Northern (Southern) Hemisphere, there are two (one) zones of negative declinations ($D$) and two (one) zones of positive declination angles ($D$). $\Delta V_y$ correspondingly shows two positive and negative zones
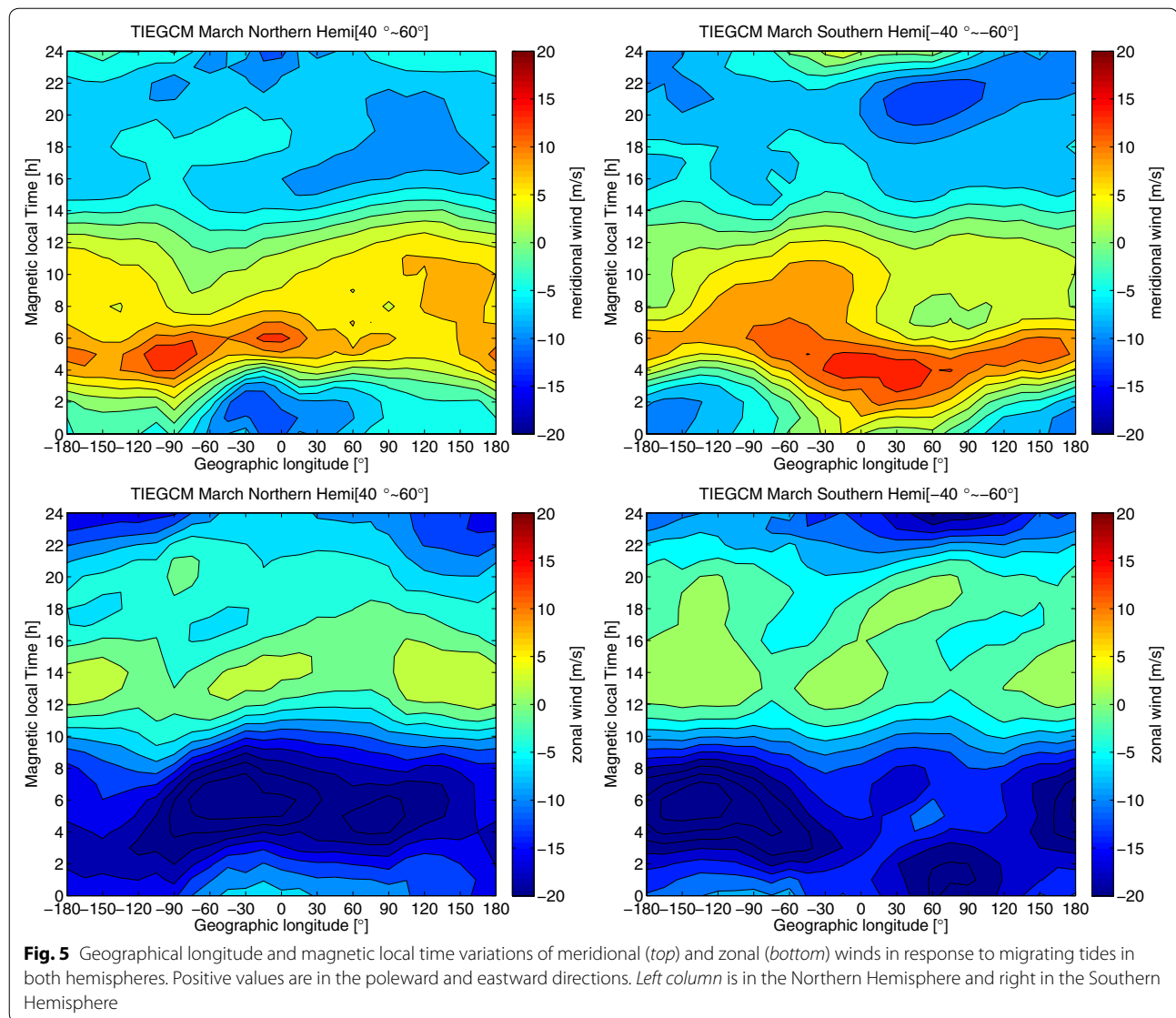
**Fig. 3** Vertical and longitudinal variations of the residual electron density (ΔNe) due to migrating tidal effects at different magnetic local time in both hemispheres. δΔNe is got by differentiating two runs with and without migrating tidal inputs at the low boundary of model. *Top panels* show the absolute differences given in $10^{10}$ m$^{-3}$, and *bottom panels* show the relative difference given in percent

because of $\sin D$ (see the top of Fig. 6). The tidal zonal wind is westward in the pre-noon and evening sectors, while negligible in the post-noon sectors. The westward zonal wind causes two bands of upward and downward movement of the plasma in the Northern Hemisphere and one band of upward and downward motion of the plasma in the Southern Hemisphere (see top of Fig. 6). When the plasma is moved upward to the low recombination region, the plasma density becomes enhanced, and vice versa. When we compare $\Delta V_y$ with the $\Delta Ne$ (Fig. 6 vs. Fig. 4), we find that the upward (downward) plasma motion coincides with the enhanced (reduced) $\Delta Ne$ except for a 4-h time delay. This confirms that the tidal zonal wind effect on the $\Delta Ne$ is through the vertical motion of the plasma along the magnetic field.

The middle portion of Fig. 4 shows the effect of tidal meridional wind on the $\Delta Ne$. There is one obvious peak and trough (wave-1 structure) along the longitude in both hemispheres. The wave phase is nearly reversed in both hemispheres. The tidal meridional wind acts in almost an opposite way to the zonal wind over NA and in the Southern Hemisphere. Moreover, the meridional wind effect is stronger than the zonal wind in the Northern Hemisphere, while weaker in the Southern Hemisphere. Thus, the total wind effects (as shown at the bottom of Fig. 4) more closely resemble meridional wind in the Northern Hemisphere and zonal wind, except for the daytime, in the Southern Hemisphere. The tidal meridional wind effect on the $\Delta Ne$ is also evidenced through the vertical transport of plasma. As shown in the middle
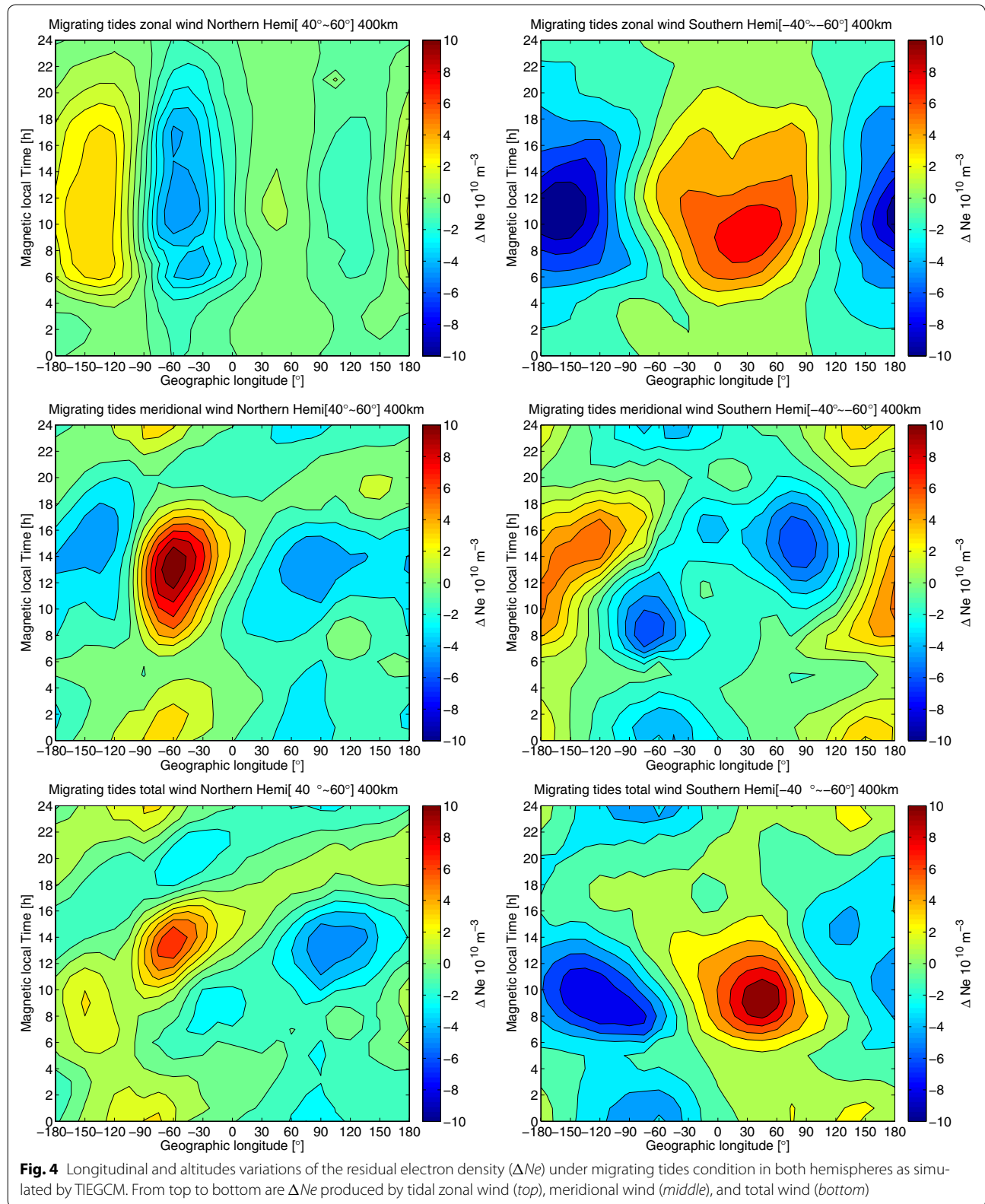
**Fig. 4** Longitudinal and altitudes variations of the residual electron density (Δ*Ne*) under migrating tides condition in both hemispheres as simulated by TIEGCM. From top to bottom are Δ*Ne* produced by tidal zonal wind (*top*), meridional wind (*middle*), and total wind (*bottom*)
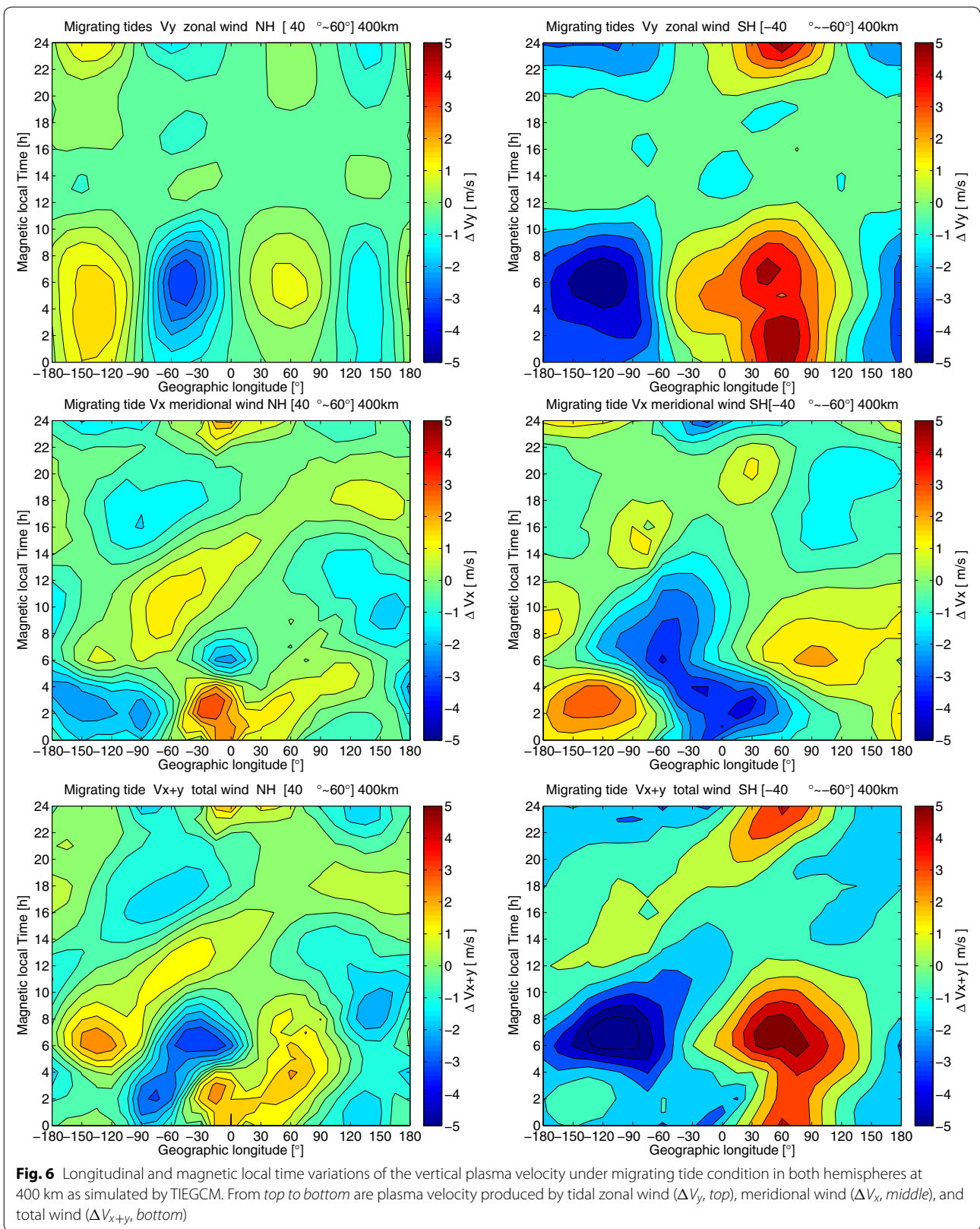
**Fig. 5** Geographical longitude and magnetic local time variations of meridional (*top*) and zonal (*bottom*) winds in response to migrating tides in both hemispheres. Positive values are in the poleward and eastward directions. *Left column* is in the Northern Hemisphere and right in the Southern Hemisphere

of Fig. 6, the vertical velocity due to the tidal meridional wind $(V_x = U_x \cos D \cos |I| \sin |I| = \frac{1}{2} U_x \cos D \sin 2I)$ is consistent with the $\Delta Ne$ except for a time delay of 4 h. $V_x$ is larger than $V_y$ in the Northern Hemisphere and smaller in the Southern Hemisphere. Thus, $\Delta V_{x+y}$ more closely resembles $\Delta V_x$ in the Northern Hemisphere and $\Delta V_y$ in the Southern Hemisphere (see the bottom of Fig. 6).

The non-wind effect constitutes a major charge of the $\Delta Ne$ under migrating tidal input, which is shown at the top of Fig. 7. Its effect on the $\Delta Ne$ is nearly 180° out of phase to the tidal wind. The differences between the peak and trough of the $\Delta Ne$ are calculated for quantitative comparison. The tidal non-wind processes provide about 64% of the contributions, while the neutral wind

accounts for approximately 36% in the Northern Hemisphere. In the Southern Hemisphere, the tidal wind effect is the opposite to that of the tidal non-wind effect. The neutral composition ratio $\Delta O/N_2$ shown at the bottom of Fig. 7 exhibits a similar structure to the $\Delta Ne$ driven by non-wind processes. This confirms that the neutral composition change is one of potential candidates in disturbing the $\Delta Ne$ under migrating tidal conditions.

Another point needs to be addressed here. By using the GITM model, Wang and Liu (2015) showed an enhanced $\Delta Ne$ wave in NA (180°W−0° GLon) produced by an upward-propagating migrating tide when compared to those caused by in situ processes. However, the TIEGCM shows a reduced $\Delta Ne$ wave in the NA sector (see the left-hand side of the bottom panel in Fig. 2). The reason for
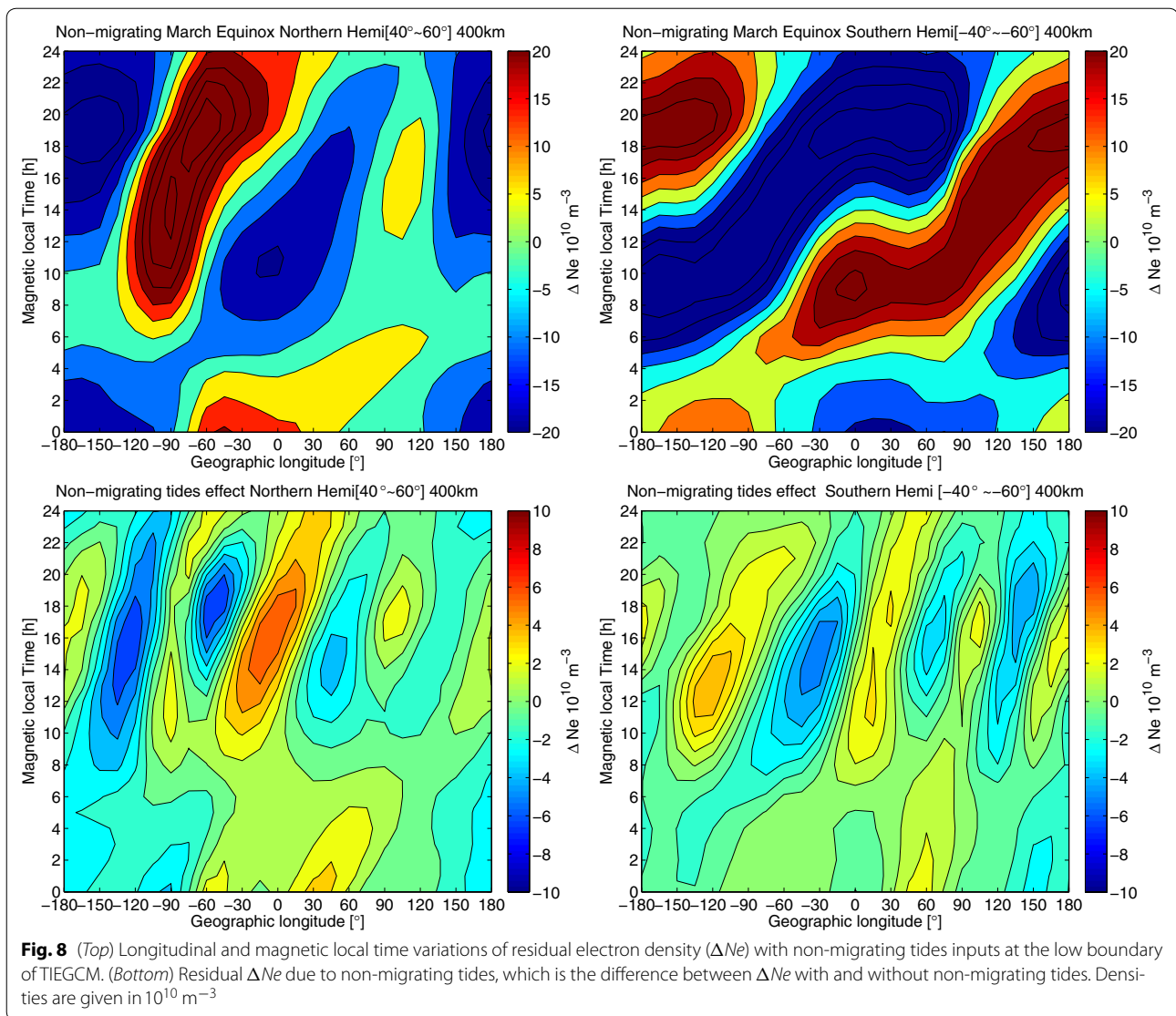
**Fig. 6** Longitudinal and magnetic local time variations of the vertical plasma velocity under migrating tide condition in both hemispheres at 400 km as simulated by TIEGCM. From *top to bottom* are plasma velocity produced by tidal zonal wind ($\Delta V_y$, *top*), meridional wind ($\Delta V_x$, *middle*), and total wind ($\Delta V_{x+y}$, *bottom*)

**Fig. 7** Longitudinal and magnetic local time variations in the residual electron density ($\Delta Ne$) driven by migrating tidal non-wind effects (*top*), and the ratio between Oxygen and Nitrogen ($\Delta O/N_2$) at 400 km in both hemispheres (*bottom*)

this contradiction is that the GITM only includes the tidal wind, but excludes the tidal neutral compositions in the coupling between the lower atmosphere and thermosphere, while the TIEGCM includes both disturbances in the lower and upper atmosphere coupling.

### Non-migrating tidal effects

The top of Fig. 8 shows the variation of $\Delta Ne$ simulated with non-migrating tides imposed at the lower boundary of the model in both hemispheres. The $\Delta Ne$ pattern is the same as that without non-migrating tidal inputs (i.e., the $\Delta Ne$ driven by in situ processes as shown in Fig. 1). This indicates that upward-propagating non-migrating tides play a minor role in the modulation of the $\Delta Ne$ as compared to in situ processes.

The residual $\Delta Ne$, due to lower atmosphere non-migrating tides, is shown at the bottom of Fig. 8. It was

obtained by differentiating two runs with and without non-migrating tidal inputs at the lower boundary. This demonstrates a wave-4 structure of the $\Delta Ne$ in both hemispheres. The amplitudes are similar but become reduced at mid-latitudes, when compared to the well-known wave-4 pattern in equatorial regions (figure not shown). The amplitude ratio between the mid-latitude and equator regions is about 32% (22%) in the Northern (Southern) Hemisphere. In both hemispheres, the longitudinal structure of the $\Delta Ne$ at mid-latitudes is nearly out of phase with those in the equatorial regions. Four peaks were found at: 180°E, 90°W, 15°W, and 90°E in the Northern Hemisphere, and at: 135°W, 15°E, 100°E, and 180°E in the Southern Hemisphere. The altitudinal and longitudinal variation of the residual $\Delta Ne$ in 14 MLT are shown in Fig. 9. The longitudinal differences are weak at altitudes below 200 km, while the relative variation is

**Fig. 8** (*Top*) Longitudinal and magnetic local time variations of residual electron density (Δ*Ne*) with non-migrating tides inputs at the low boundary of TIEGCM. (*Bottom*) Residual Δ*Ne* due to non-migrating tides, which is the difference between Δ*Ne* with and without non-migrating tides. Densities are given in $10^{10}$ m$^{-3}$

apparent. An obvious wave-4 structure appeared in both hemispheres with a maximum at around 300 km, indicative of the direct penetration of the non-migrating tidal effect into the E and F layers ionosphere.

The non-migrating tidal effect is divided into two groups: tidal wind and non-wind. Six runs are conducted for further investigation in a similar way as that conducted on the migrating tides. The non-migrating tidal effects on winds are shown in Fig. 10. Both meridional and zonal winds exhibit wave-4 patterns in both hemispheres. Figure 11 shows the tidal zonal, meridional, and total wind effects on the Δ*Ne*. A wave-1 structure of the Δ*Ne* existed, which is induced by the tidal zonal wind with phase reversed in the Northern and Southern Hemispheres (see the top of Fig. 11). A wave-4 and wave-2 structure of the Δ*Ne*, due to meridional wind, exists in

the Northern and Southern Hemispheres (refer to the second row in Fig. 11). The structure of the Δ*Ne*, due to total wind (see the third row in Fig. 11), was quite similar to the meridional wind in both hemispheres. The vertical transport of plasma due to neutral winds, $\Delta VV_{x+y}$, is consistent with the Δ*Ne* caused by the neutral winds (see the bottom of Fig. 11). This shows that the tidal neutral winds work on the *Ne* mainly through the vertical transport along the magnetic field.

The tidal non-wind effect is in major charge of the Δ*Ne* under non-migrating tidal input, which is shown at the top of Fig. 12. For the non-migrating tides, the wind effect is opposite to the non-wind effect. The neutral composition ratio $\Delta O/N_2$ is shown at the bottom of Fig. 12, which exhibits a similar structure to the Δ*Ne* driven by non-wind processes. This confirms that the neutral

**Fig. 9** The same as Fig. 3, but for non-migrating tidal conditions
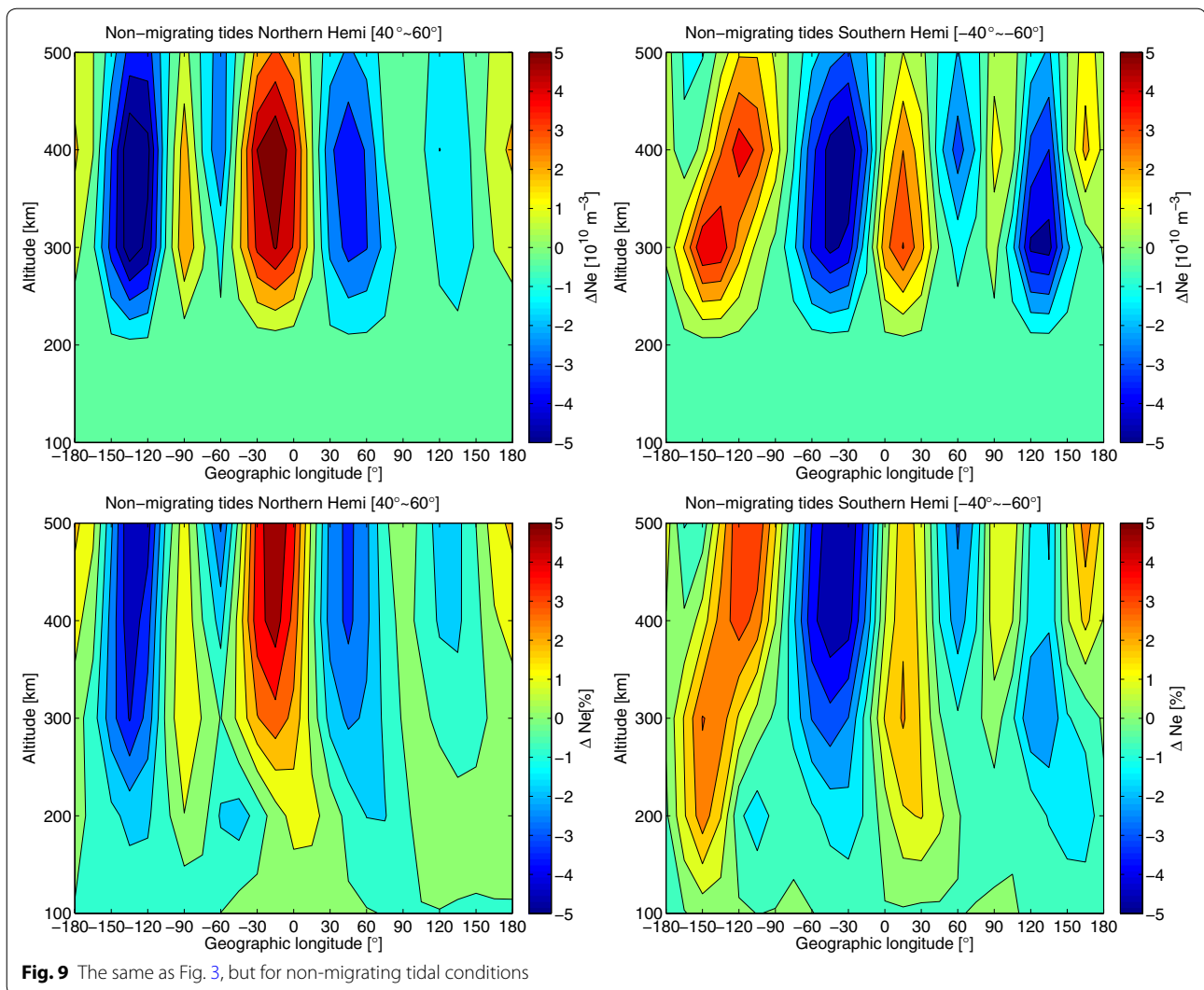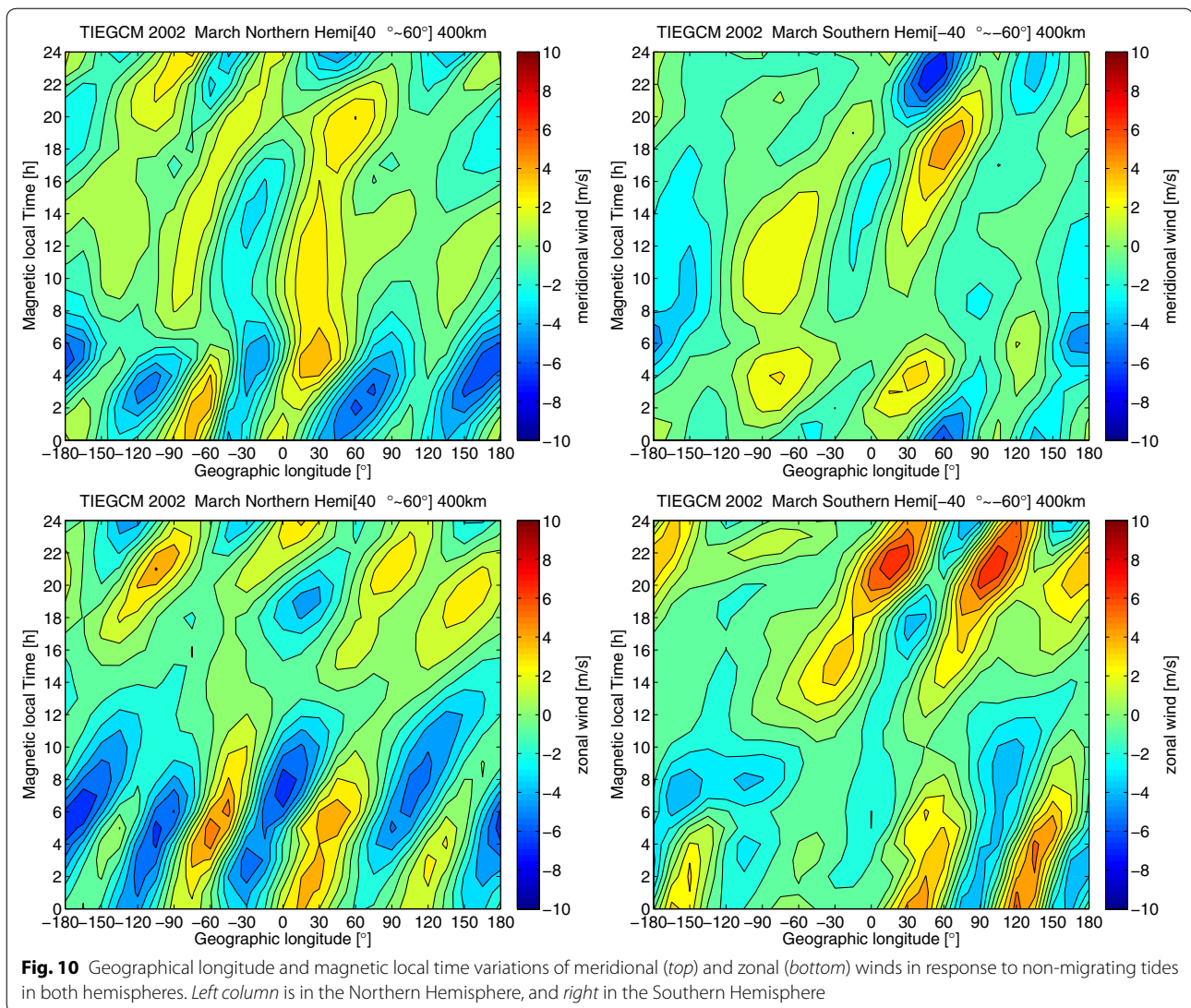
composition ratio is one of potential candidates in disturbing the $\Delta Ne$ under non-migrating tidal conditions.

**Tidal decomposition**

The quantitative contribution from the lower atmosphere to the $\Delta Ne$ at F region, as described earlier in our introduction, is not completely understood. To further understand this phenomenon, we performed tidal diagnostics of the $\Delta Ne$ at F region for three cases. The major non-migrating tidal components are listed in Table 1. The case with no tide represents the local physical process effects, in comparison with those from migrating and non-migrating tides.

The two major tidal components, under no tidal input conditions, are D0 and DE1 in the Northern Hemisphere, and D0 and DW2 in the Southern Hemisphere. Those

are listed in bold in Table 1. With migrating tidal input, D0 and DE1 can be enhanced by 8% and 3%, respectively, in the Northern Hemisphere, whereas D0 and DW2 can be enhanced by 13% and 21%, respectively, in the Southern Hemisphere. With non-migrating tidal input, D0 and DE1 are enhanced by 3% and 10%, respectively, in the Northern Hemisphere, whereas D0 and DW2 are enhanced by 3% and 2%, respectively, in the Southern Hemisphere. These represent the quantitative contribution from the lower atmosphere to the $\Delta Ne$ in the F region. It can be seen that the DW2 and D0 components are less affected by non-migrating tides from lower atmosphere, which is most likely generated in situ by nonlinear interaction forcing in the upper thermosphere. This is consistent with the conclusion by Oberheide et al. (2011) who present a climatological tidal model of the

**Fig. 10** Geographical longitude and magnetic local time variations of meridional (*top*) and zonal (*bottom*) winds in response to non-migrating tides in both hemispheres. *Left column* is in the Northern Hemisphere, and *right* in the Southern Hemisphere

thermosphere (CTMT) of upward-propagating migrating and non-migrating diurnal and semidiurnal tides from 80–400 km and pole to pole. This is based on Hough Mode Extension fits to 2002–2008 TIMED satellite tidal diagnostics in the lower thermosphere. They validated the CTMT with CHAMP tidal diagnostics at around 400 km. Their results proved that the theoretical model captured the observed non-migrating tides well, indicating that these waves propagate directly upward without significant weakening. The exceptions are the DW2 and D0 components, which are believed to be most likely generated in situ by nonlinear interaction forcing in the upper thermosphere.

## Conclusions

This study investigates the upward-propagating migrating and non-migrating tidal effects from the lower

atmosphere on the longitudinal variation of electron density ($\Delta Ne$) at mid-latitudes during March equinox. Twelve runs, using TIEGCM for investigation, are conducted. The $\Delta Ne$ at altitudes above 200 km are affected by upward-propagating tides. Migrating tides result in reduced longitudinal differences in the $\Delta Ne$ over North America and in the Southern Hemisphere. Non-migrating tides result in a wave-4 structure of the $\Delta Ne$ in both hemispheres, but with weaker amplitudes as compared to migrating tides. The neutral composition changes play dominant roles in regulating the $\Delta Ne$ under both migrating (accounting for about 64%) and non-migrating (approximately 60%) tidal conditions, which oppose the tidal wind effects. The $\Delta Ne$ driven by tidal meridional wind (accounting for about 70%) is stronger than tidal zonal wind (approximately 30%) under both migrating and non-migrating tidal
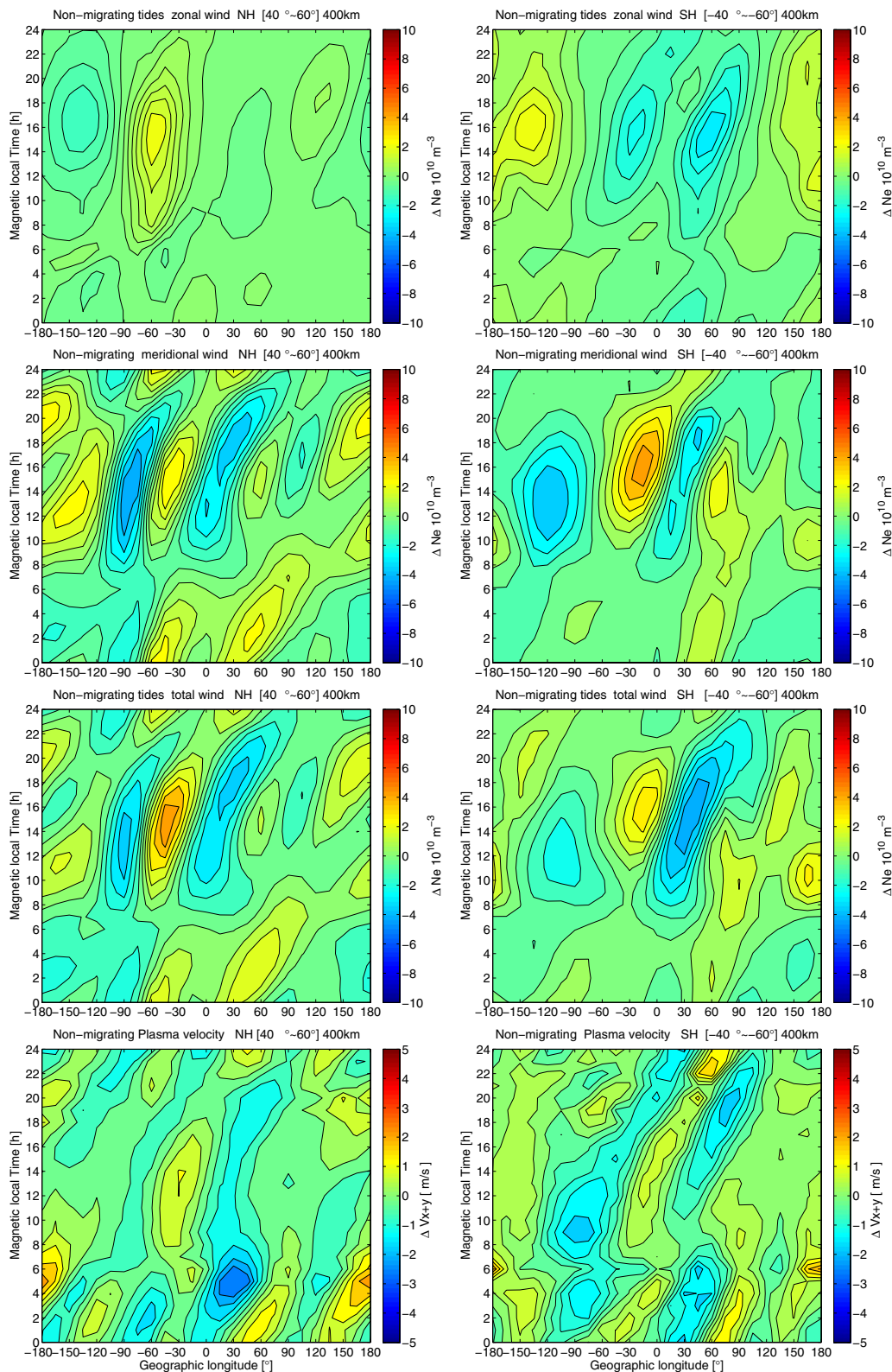
**Fig. 11** Longitudinal and altitudes variations of the residual electron density (ΔNe) under non-migrating tide condition in both hemispheres as simulated by TIEGCM. From top to bottom are ΔNe due to tidal zonal wind (*top*), meridional wind (*second row*), total wind (*third row*), and plasma vertical velocity due to tidal wind (*bottom*)

**Fig. 12** Longitudinal and magnetic local time variations in the residual electron density ($\Delta Ne$) driven by non-wind effects under non-migrating tide condition (*top*), and the ratio between Oxygen and Nitrogen ($\Delta O/N_2$) at 400 km in both hemispheres (*bottom*)
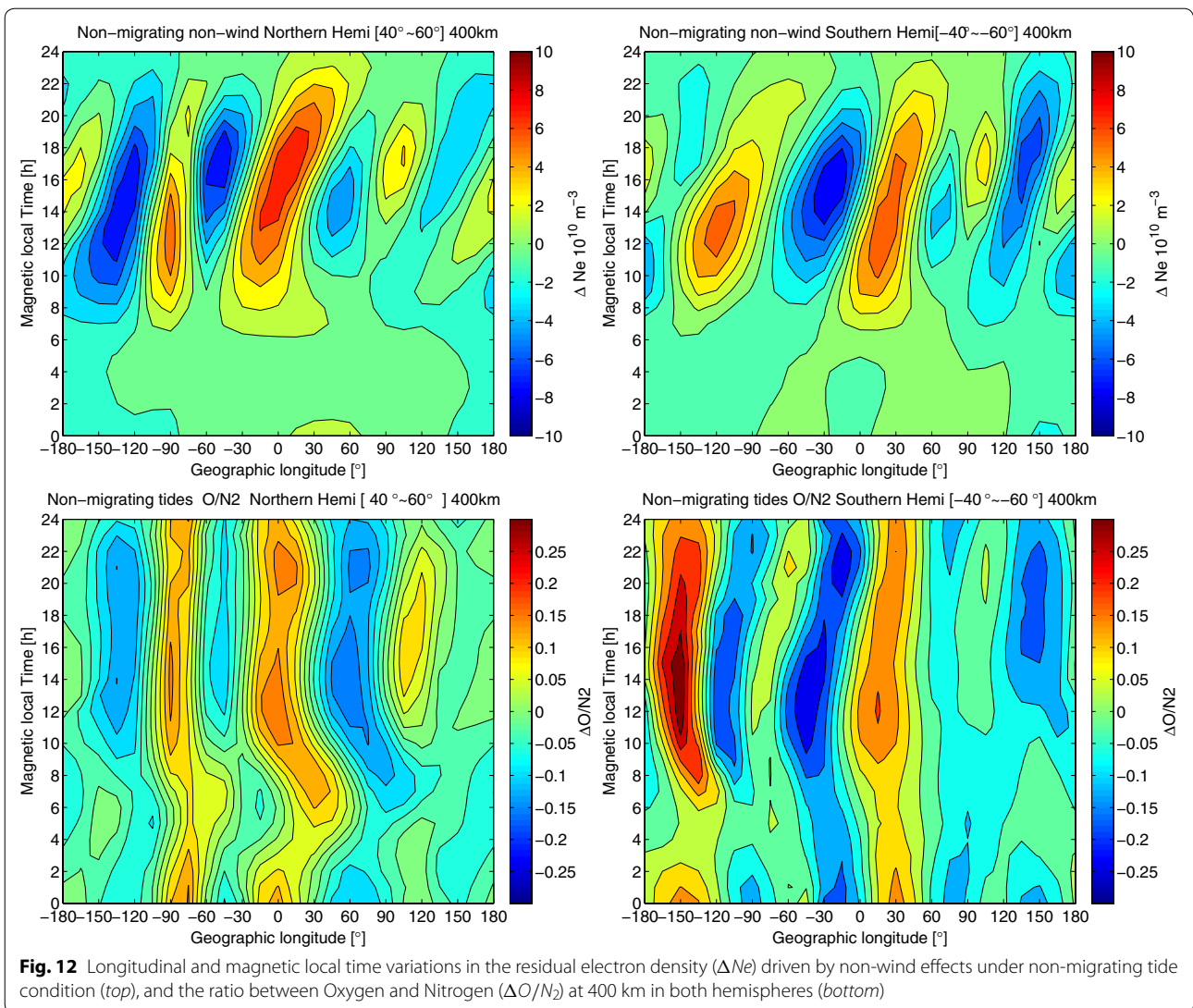
**Table 1 Tidal decomposition of $\Delta Ne$ for three conditions in the Northern and Southern Hemispheres**

| Northern Hemisphere | | | | | | Southern Hemisphere | | | | | |
|---|---|---|---|---|---|---|---|---|---|---|---|
| | No tide | Migrating tide | | Non-migrating tide | | | No tide | Migrating tide | | Non-migrating tide | |
| | A | A | R (%) | A | R (%) | | A | A | R (%) | A | R (%) |
| D0 | 11.0 | 0.9 | 8 | 0.3 | 3 | D0 | 23.0 | 3.1 | 13 | 0.8 | 3 |
| DE1 | 12.0 | 0.4 | 3 | 1.2 | 10 | DW2 | 11.7 | 2.4 | 21 | 0.2 | 2 |
| DE3 | 2.3 | 0.2 | 9 | 1.4 | 61 | DE2 | 2.9 | 0.2 | 7 | 0.9 | 31 |

The case without tide represents in situ physical process. The other two cases represent effects from migrating and non-migrating tides from lower atmosphere. 'A' stands for 'absolute' and 'R' stands for 'relative'

conditions, except for the southern hemisphere under migrating tidal input.

### References

Brahmanandam P, Chu YH, Wu KH, Hsia HP, Su CL, Uma G (2011) Vertical and longitudinal electron density structures of equatorial E- and F-regions. Ann Geophys 29:81–89. doi:10.5194/angeo-29-81-2011

Chang LC, Liu H, Miyoshi Y, Chen CH, Chang FY, Lin CH, Sun YY (2015) Structure and origins of the Weddell Sea Anomaly from tidal and planetary wave signatures in FORMOSAT-3/COSMIC observations and GAIA GCM simulations. J Geophys Res 120(2):1325–1340. doi:10.1002/2014JA020752

Chen CH, Lin CH, Chang LC, Huba JD, Lin JT, Satio A, Liu JY (2013) Thermospheric tidal effects on the ionospheric midlatitude summer nighttime anomaly using SAMI3 and TIEGCM. J Geophys Res 118(6):3836–3845. doi:10.1002/jgra.50340

Dickinson R, Ridley E, Roble R (1984) Thermospheric general circulation with coupled dynamics and composition. J Atoms Sci 41:205–219. doi:10.1175/1520-0469(1984)041h0205:TGCWCDi2.0.CO;2

Emery B, Coumans V, Evens D, Germany G, Greer M, Holeman E, Kadinsky-Cade K, Rich F, Xu W (2008) Seasonal, Kp, solar wind, and solar flux variations in long-term singlepass satellite estimates of electron and ion auroral hemispheric power. J Geophys Res 113(A06):311. doi:10.1029/2007JA012866

England SL (2012) A review of the effects of non-migrating atmospheric tides on the earth's low-latitude ionosphere. Space Sci Rev 168(1–4):211–236. doi:10.1007/s11214-011-9842-4

England SL, Immel T, Sagawa E, Henderson S, Hagan M, Mende S, Frey H, Swenson C, Paxton L (2006a) Effect of atmospheric tides on the morphology of the quiet time, postsunset equatorial ionospheric anomaly. J Geophys Res 111:A10S19. doi:10.1029/2006JA011795

England SL, Maus S, Immel TJ, Mende SB (2006b) Longitudinal variation of the E-region electric fields caused by atmospheric tides. Geophys Res Lett 33:L21105. doi:10.1029/2006GL027465

England SL, Zhang X, Immel TJ, Forbes J, DeMajistre R (2009) The effect of non-migrating tides on the morphology of the equatorial ionospheric anomaly: seasonal variability. Earth Planets Space 61(4):493–503. doi:10.1186/BF03353166

England SL, Immel TJ, Huba JD, Hagan ME, Maute A, Demajistre R (2010) Modeling of multiple effects of atmospheric tides on the ionosphere: an examination of possible coupling mechanisms responsible for the longitudinal structure of the equatorial ionosphere. J Geophys Res 115(A5):511–535. doi:10.1029/2009JA014894

Fang TW, Kil H, Millward G, Richmond AD, Liu JY, Oh SJ (2009) Causal link of the wave-4 structures in plasma density and vertical plasma drift in the low-latitude ionosphere. J Geophys Res 114(A10):125–134. doi:10.1029/2009JA014460

Hagan ME, Forbes JM (2002) Migrating and nonmigrating diurnal tides in the middle and upper atmosphere excited by tropospheric latent heat release. J Geophys Res 107:4754. doi:10.1029/2001JD001236

Hagan ME, Forbes JM (2003) Migrating and nonmigrating semidiurnal tides in the upper atmosphere excited by tropospheric latent heat release. J Geophys Res 108:1062. doi:10.1029/2002JA009466

Hagan ME, Maute A, Roble RG, Richmond AD, Immel TJ, England SL (2007) Connections between deep tropical clouds and the Earth's ionosphere. Geophys Res Lett. doi:10.1029/2007GL030142

Häusler K, Lühr H (2009) Nonmigrating tidal signals in the upper thermospheric zonal wind at equatorial latitudes as observed by CHAMP. Ann Geophys 27:2643–2652. doi:10.5194/angeo-27-2643-2009

Heelis R, Winningham J, Hanson W, Burch J (1980) The relationships between high-latitude convection reversals and the energetic particle morphology observed by atmosphere explorer. J Geophys Res 85:3315–3324. doi:10.1029/JA085iA07p03315

Heelis R, Lowell J, Spiro R (1982) A model of the high-latitude ionospheric convection pattern. J Geophys Res 87(A3):6339–6345. doi:10.1029/JA087iA08p06339

Henderson SB, Swenson CM, Gunther JH, Christensen AB, Paxton LJ (2005) Method for characterization of the equatorial anomaly using image subspace analysis of global ultraviolet imager data. J Geophys Res. doi:10.1029/2004JA010830

Heroux L, Higgins J (1977) Summary of full disk solar fluxes between 250 and 1940 A. J Geophys Res 82:3307–3310. doi:10.1029/JA082i022p03307

Heroux L, Hinteregger H (1978) Aeronomical reference spectrum for solar UV below 2000 Å. J Geophys Res 83:5305–5308. doi:10.1029/JA083iA11p05305

Immel TJ, Sagawa E, England SL, Henderson SB, Hagan ME, Mende SB, Frey HU, Swenson CM, Paxton LJ (2006) Control of equatorial ionospheric morphology by atmospheric tides. Geophys Res Lett 33:L15108. doi:10.1029/2006GL026161

Jin H, Miyoshi Y, Fujiwara H, Shinagawa H (2008) Electrodynamics of the formation of ionospheric wave number 4 longitudinal structure. J Geophys Res. doi:10.1029/2008JA013301

Jones J, Forbes JM, Hagan ME, Maute A (2013) Non-migrating tides in the ionosphere-thermosphere: in situ versus tropospheric sources. J Geophys Res 118:2438–2451. doi:10.1002/jgra.50527

Kil H, Talaat E, Oh SJ, Paxton L, England S, Su SJ (2008) Wave structures of the plasma density and E × B drift in low-latitude F region. J Geophys Res 113(A09):312. doi:10.1029/2008JA013106

Kil H, Kwak YS, Lee WK, Krall J, Huba JD, Oh SJ (2015) Nonmigrating tidal signature in the distributions of equatorial plasma bubbles and prereversal enhancement. J Geophys Res 120:3254–3262. doi:10.1002/2014JA020908

Kwak YS, Kil H, Lee WK, Oh SJ, Ren Z (2012) Nonmigrating tidal characteristics in thermospheric neutral mass density. J Geophys Res 117(117):1–2. doi:10.1029/JA016932

Laskar FI, Chau JL, Stober G, Hoffmann P, Hall CM, Tsutsumi M (2016) Quasi-biennial oscillation modulation of the middle- and high-latitude mesospheric semidiurnal tides during August–September. J Geophys Res Space Physics 121:48694879. doi:10.1002/2015JA02206

Lin CH, Wang W, Hagan ME, Hsiao CC, Immel TJ, Hsu ML, Liu JY, Paxton LJ, Fang TW, Liu CH (2007) Plausible effect of atmospheric tides on the equatorial ionosphere observed by the formosat-3/cosmic: three-dimensional electron density structures. Geophys Res Lett. doi:10.1029/2007GL029265

Liu H, Mamoru Y, Hermann L (2009) Wave-4 pattern of the equatorial mass density anomaly: a thermospheric signature of tropical deep convection. Geophys Res Lett 36(18):120–131. doi:10.1029/2009GL039865

Lühr H, Häusler K, Stolle C (2007) Longitudinal variation of F region electron density and thermospheric zonal wind caused by atmospheric tides. Geophys Res Lett 34(16):102. doi:10.1029/2007GL030639

Mukhtarov P, Pancheva D (2011) Global ionospheric response to nonmigrating DE3 and DE2 tides forced from below. J Geophys Res 116(A05):323. doi:10.1029/2010JA016099

Nogueira P, Abdu M, Souza J, Bailey G, Batista I, Shume I, Denardini C (2013) Longitudinal variation in Global Navigation Satellite Systems TEC and topside ion density over South American sector associated with the four-peaked wave structures. J Geophys Res 118:7940–7953. doi:10.1002/2013JA019266

Oberheide J, Wu Q, Killeen TL, Hagan ME, Roble RG (2006) Diurnal nonmigrating tides from TIMED Doppler Interferometer wind data: monthly climatologies and seasonal variations. J Geophys Res 111:A10S03. doi:10.1029/2005JA011491

Oberheide J, Forbes JM, Häusler K, Wu Q, Bruinsma SL (2009) Tropospheric tides from 80 to 400 km: propagation, interannual variability, and solar cycle effects. J Geophys Res 114(D1):D00,105. doi:10.1029/2009JD012388

Oberheide J, Forbes JM, Zhang X, Bruinsma SL (2011) Climatology of upward propagating diurnal and semidiurnal tides in the thermosphere. J Geophys Res 116:A11306. doi:10.1029/2011JA016784

Pedatella N, Hagan M, Maute A (2012) The comparative importance of DE3, SE2, and SPW4 on the generation of wavenumber-4 longitude structures in the low-latitude ionosphere during September equinox. Geophys Res Lett 39(L19):108. doi:10.1029/2012GL053643

Pedatella NM, Forbes JM, Oberheide J (2008) Intra-annual variability of the low-latitude ionosphere due to nonmigrating tides. Geophys Res Lett 35(18):60–74. doi:10.1029/2008GL035332

Reigber C, Luehr H, Schwintzer P (2002) CHAMP mission status. Adv Space Res 30(2):129–134. doi:10.1016/S0273-1177(02)00276-4

Ren Z, Wan W, Liu L, Xiong J (2009) Intra-annual variation of wave number 4 structure of vertical E ×B drifts in the equatorial ionosphere seen from ROCSAT-1. J Geophys Res. doi:10.1029/2009JA014060

Ren Z, Wan W, Xiong J, Liu L (2010) Simulated wave number 4 structure in equatorial f-region vertical plasma drifts. J Geophys Res. doi:10.1029/2009JA014746

Richards PG, Fennelly JA, Torr DG (1994) A solar euv flux model for aeronomic calculations. J Geophys Res 99(A5):8981–8992. doi:10.1029/94JA00518

Sagawa E, Immel T, Frey H, Mende S (2005) Longitudinal structure of the equatorial anomaly in the nighttime ionosphere observed by IMAGE/FUV. J Geophys Res 110(A11):302. doi:10.1029/2004JA010848

Scherliess L, Thompson DC, Schunk RW (2008) Longitudinal variability of low-latitude total electron content: tidal influences. J Geophys Res 113:A01311. doi:10.1029/2007JA012480

Wan W, Liu L, Pi X, Zhang ML, Ning B, Xiong J, Ding F (2008) Wavenumber-4 patterns of the total electron content over the low latitude ionosphere. Geophys Res Lett 35(L12):104. doi:10.1029/2008GL033755

Wang H, Liu DW (2015) Tidal spectrum analysis of electron density and plasma vertical velocity at mid-latitudes. Chin J Geophys. doi:10.1360/N972015-00256

Wang H, Ridley AJ, Zhu J (2015) Theoretical study of zonal differences of electron density at midlatitudes with GITM simulation. J Geophys Res 120(4):2951–2966. doi:10.1002/2014JA020790

Wang H, Liu D, Zhang J (2016) Vertical structure of longitudinal differences in electron densities at mid-latitudes. Sci Bull 61(3):252–262. doi:10.1007/s11434-015-0993-7

Wu Q, Ortland DA, Foster B, Roble RG (2012) Simulation of nonmigrating tide influences on the thermosphere and ionosphere with a TIMED data driven TIEGCM. J Atmos Sol Terr Phys 90:61–67. doi:10.1016/j.jastp.2012.02.009

Xiong C, Lühr H (2014) The Midlatitude Summer Night Anomaly as observed by CHAMP and GRACE: Interpreted as tidal features. J Geophys Res 119:4905–4915. doi:10.1002/2014JA019959

Xu JS, Li XJ, Yw Liu, Jing M (2013) TEC differences for the mid-latitude ionosphere in both sides of the longitudes with zero declination. Adv Space Res 54(5):883–895. doi:10.1016/j.asr.2013.01.010

Zhang SR, Foster JC, Coster AJ, Erickson PJ (2011) East-West Coast differences in total electron content over the continental US. Geophys Res Lett 38:L19101. doi:10.1029/2011GL049116

Zhang X, Forbes JM, Hagan ME (2010) Longitudinal variation of tides in the MLT region: 2. Relative effects of solar radiative and latent heating. J Geophys Res 115:A06317. doi:10.1029/2009JA014898

Zhao B, Wang M, Wang Y, Ren Z, Yue X, Zhu J, Wan W, Ning B, Liu J, Xiong B (2013) East-west differences in F-region electron density at midlatitude: evidence from the Far East region. J Geophys Res 118:542–553. doi:10.1029/2012JA018235